Structural Engineering and Mechanics, *Vol. 60, No. 6 (2016) 1079-1092*
DOI: http://dx.doi.org/10.12989/sem.2016.60.6.1079

Displacements of the flexible ring for an electromechanical integrated harmonic piezodrive system

Lizhong Xu*, Huaiyong Li[a] and Chong Li[b]

Mechanical Engineering Institute, Yanshan University, Qinhuangdao 066004, China

(Received May 10, 2014, Revised August 25, 2016, Accepted October 12, 2016)

Abstract. In this paper, an electromechanical integrated harmonic piezodrive system is proposed. The operating principle of the drive system is introduced. The equation of the relationship between the displacements of the flexible ring and the rotating angle of the rotor is deduced. Using the equation, the displacements of the flexible ring for the drive system and their changes along with the system parameters are investigated. The results show that the displacements of the flexible ring changes periodically along with the rotation of the vibrator; there are abrupt changes in the displacements of the flexible ring at some points where there are abrupt changes in the number of the mesh teeth pair; the length of the flexible ring, the excitation voltage, and the speed ratio have obvious effects on the displacements of the flexible ring. The results are useful for the design of the drive system.

Keywords: electromechanical integrated; piezodrive; flexible ring; Displacement; harmonic drive; movable tooth

1. Introduction

Ultrasonic piezoelectric actuators and their related devices are currently used in many industries and research fields. Compared with the conventional electromagnetic motors, they offer many prominent advantages such as small size, stable operation with low velocity and high torque, no magnetic disturbance, quick response, etc.

Sashida (1982, 1984) developed a standing wave ultrasonic motor and a traveling-wave ultrasonic motor. Based on traveling-wave ultrasonic motor proposed by Sashida, Ishe proposed a ring-shaped traveling-wave ultrasonic motor in which the teeth were manufactured on the vibrator. It enlarged the vibrating amplitudes of the vibrator and the motor efficiency was increased (Tokushima and Harao 1987). Using analytic method combined with numerical method, an analysis and design method for the ultrasonic motors was proposed, and the proposed analysis and design method was validated by comparing its outcomes with the experimental data (Rho, Lee *et al*. 2008). A number of the control methods were proposed for the ultrasonic motor (Hieu, Odomari *et al*. 2013, Shi and You 2014).

*Corresponding author, Professor, E-mail: xlz@ysu.edu.cn
[a]Ph.D., E-mail: lihuaiyong@ysu.edu.cn
[b]Ph.D. Student, E-mail: lichong1237@126.com

http://www.techno-press.org/?journal=sem&subpage=8 ISSN: 1225-4568 (Print), 1598-6217 (Online)

However, the friction drive between the stator and the rotor is a weak link of the piezoelectric motors which limits the output torque and the operating life. Hence, Yamayoshi (1992) proposed a non-contact ultrasonic motor in which the fluid between the stator and the rotor is used to transmit torque and a speed of 3000rpm was obtained under the excitation voltage of 100V. Ueha (2000) proposed a non-contact ultrasonic linear motor which can move the weight of 8.6g at a velocity of 0.7m/s. Yang (2006) investigated a micro non-contact ultrasonic motor based on B22 vibration mode in which the rotor speed of 3569 rpm was given at the input voltage of 20 V and the driving frequency of 45.6 kHz. Hojjat (2010) proposed a rolling-contacting ultrasonic motor in which the rollers are located between the grooves of stator, and the elliptical motion of the stator surface causes the rollers to rotate, and the rollers drive the rotor to rotate. Stepanenko (2012) presented a novel non-contact rotary ultrasonic motor consisting of ring-shaped stator vibrating in in-plane flexural mode and rotor provided with blades which relies on the use of standing ultrasonic waves, and design and electronic control of motor is simplified.

In a word, the non-contact ultrasonic motors and the rolling-contacting ultrasonic motors have high operating life and efficiency in spite of the small output torque, and they are proper for application fields of high speed and small load. However, in the exploration of the ultrasonic motors with large output torque, there is not a realized drive type to be given yet.

Therefore, the Authors propose an electromechanical integrated harmonic piezodrive system in which the piezodrive principle is combined with the harmonic drive and the movable tooth drive principles, and a reduction ratio is realized. Compared with other piezoelectric motors, there are three main advantages: rolling contact, transmitting load by meshing, and reduction. It makes the drive system have high operating efficiency and output torque. It is possible that the piezoelectric motor operates continuously under a relatively large load.

The free vibration of the flexible ring for the drive system has been investigated (Xu and Li 2013). In the drive system, the flexible ring is a key element. Its displacements drive the total system to work. In order to design and control the drive system, the displacements of the flexible ring for the drive system should be investigated.

This study includes three parts: (1) introduction of the operating principle of the drive system; (2) deduction of the equation of the relationship between the displacements of the flexible ring and the rotating angle of the rotor; (3) study of the displacements of the flexible ring for the drive system and their changes along with the system parameters. These studies are useful for the design and control of the operating performances of the drive system.

2. Operating principle of the drive system

The configuration of the proposed electromechanical integrated harmonic piezodrive system is shown in Fig. 1, which consists of three main parts: the vibrator (stator), the harmonic movable tooth drive without wave generator, and the flexible ring between the vibrator and the movable tooth drive. Four ring-typed piezoelectric ceramics with two separated electrodes are placed in 90^0 to each other. Fig. 1(c) shows arrangement of piezoelectric elements and electrical signals applied to them. They are used to excite the bending vibrations of the vibrator in two directions vertical to each other. When two input signals with a phase difference of 90° are applied to two pairs of the ring-typed piezoelectric ceramics, the motion of the traveling wave is produced in the vibrator of the bar-type ultrasonic motor. The vibrator contacts with a flexible ring at its roof, so the motion of the traveling wave causes the periodic elastic deformation of the flexible ring. Thus, a large

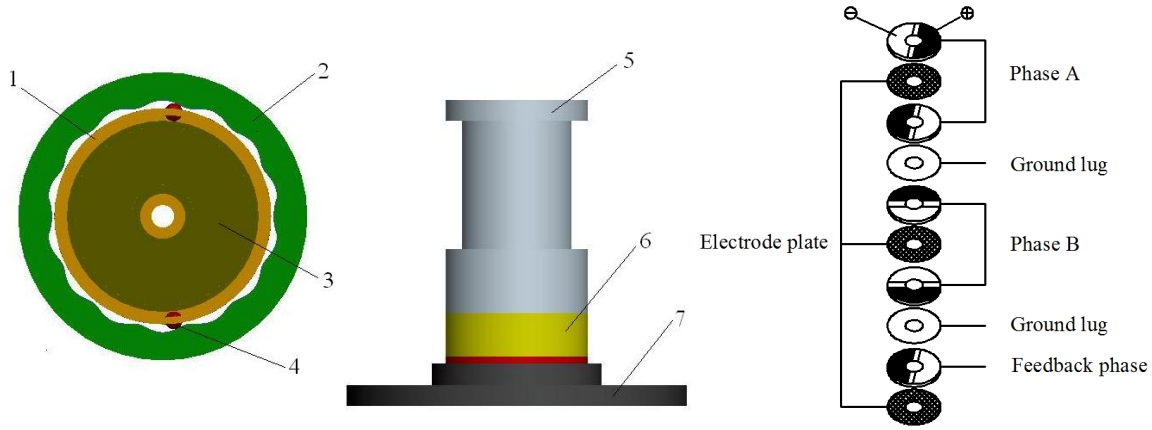

(a) Movable tooth drive (b) Stator(Vibrator) (c) Piezoelectric elements

Fig. 1 An electromechanical integrated harmonic piezodrive system, where, (1) is rotor, (2) is rigid ring, (3) is flexible ring, (4) is movable tooth, (5) is upper weight, (6) is piezoelectric ceramics, (7) is lower weight

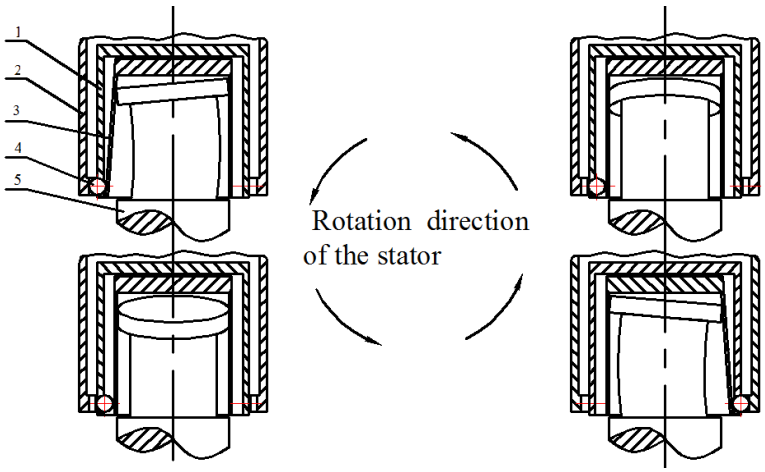

Fig. 2 The motion of the traveling wave in the vibrator and deformation of the flexible ring

periodic elastic displacement occurs at the top of the flexible ring (see Fig. 2).

The flexible ring top contacts with the movable teeth of the harmonic movable tooth drive. The periodic elastic displacement of the flexible ring top drives the movable teeth to mesh with the rigid gear, and the rotor on which the movable teeth are retained is driven to rotate. One circle of the vibrator corresponds to one tooth distance of the movable tooth motion. Hence, a reduction ratio occurs and a large output torque can be obtained.

3 The displacements of the flexible ring

A flexible ring under the force from the movable tooth is shown in Fig. 3. Compared with the radius R of the flexible ring, its thickness δ is so small that the flexible ring can be considered as

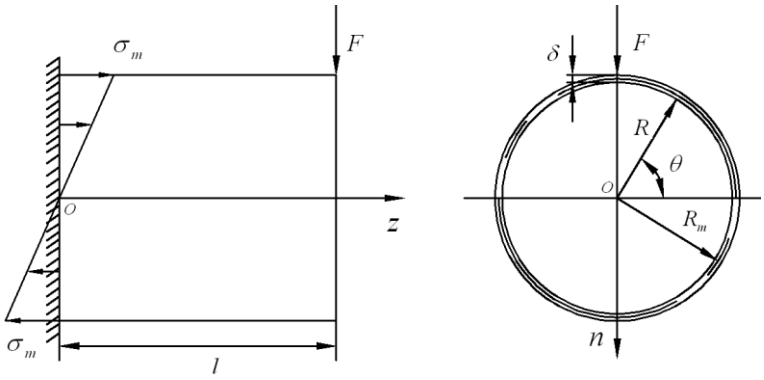

(a) The outer force on the flexible ring

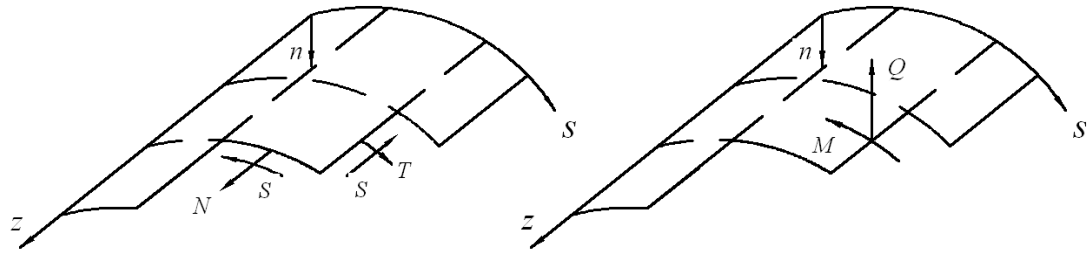

(b) Internal forces and coordinate systems of the flexible ring

Fig. 3 The force analysis model of the flexible ring

thin shell. The coordinate systems of the flexible ring are also represented in Fig. 3. The coordinate *z* is in the axial direction of the flexible ring, *n* in its radial direction, and *s* in its circumferential direction.

The flexible ring can rotate about the output shaft. The bottom of the flexible ring is quite thick by which the flexible ring is fixed on the output shaft with a roller bearing. So, for the radial displacement of the flexible ring, the bottom of the flexible ring can be considered to be fixed end.

The internal forces in the flexible ring are considered to be applied to its neutral surface as shown in Fig. 3. Here, *N* and *S* denote tensile force and shear force for unit width on the constant z section, respectively; *T* and *S* denote tensile force and shear force for unit width on the constant *s* section, respectively; *M* and *Q* denote bending moment and radial shear force for unit width on the constant *z* section, respectively.

The condition of balance for the flexible ring subjected to the force can be expressed as below

$$\left.\begin{aligned} &\frac{\partial^2(\sigma\delta)}{\partial z^2}+\Omega M=0 \\ &\Omega\sigma-\frac{E}{D\left(1-\mu^2\right)^2}\frac{\partial^2 M}{\partial z^2}=0 \end{aligned}\right\} \tag{1}$$

where $\Omega=\frac{1}{R_m^3}[\frac{\partial^4}{\partial\theta^4}+\frac{\partial^2}{\partial\theta^2}]$, σ is the normal stress on the constant *z* section, *D* is the coefficient,

$D=\dfrac{E\delta^3}{12(1-\mu^2)}$, μ is the poisson's ratio for ring material, E is the elastic modular of the flexible ring material, δ is the thickness of the flexible ring, R_m is the average radius of the flexible ring. From elastic mechanics, following relations can be given

$$\left.\begin{aligned} M &= -D\left[\frac{\partial}{\partial s}\left(\frac{\partial w}{\partial s}+\frac{v}{R}\right)+v\frac{\partial^2 w}{\partial z^2}\right] \\ \frac{\partial S}{\partial z} &= R_m\frac{\partial}{\partial s}\left(\frac{\partial^2 M}{\partial s^2}\right)+\frac{1}{R_m}\frac{\partial M}{\partial s} \\ T &= -R_m\frac{\partial^2 M}{\partial s^2} \\ Q &= \frac{\partial M}{\partial s} \end{aligned}\right\} \tag{2}$$

$$\left.\begin{aligned} \frac{\partial u}{\partial z} &= \frac{\sigma}{E}-\mu\frac{T}{E\delta} \\ \frac{\partial^2 v}{\partial z^2} &= -\frac{\partial}{\partial s}\left(\frac{\sigma}{E}-\mu\frac{T}{E\delta}\right) \\ \frac{\partial^2 w}{\partial z^2} &= -R_m\frac{\partial^2}{\partial s^2}\left(\frac{\sigma}{E}-\mu\frac{T}{E\delta}\right) \end{aligned}\right\} \tag{3}$$

The boundary conditions of the flexible ring are

$$\begin{cases} \dfrac{\partial\theta}{\partial s}=\dfrac{\partial}{\partial s}\left(\dfrac{\partial w}{\partial s}+\dfrac{v}{R}\right)=0 \\ \varepsilon_2=\dfrac{\partial v}{\partial s}-\dfrac{w}{R}=0 \\ \sigma|_{z=0}=\dfrac{Fl}{\pi R_m{}^2\delta}\sin\theta \qquad (z=0) \\ w|_{z=0}=\dfrac{\partial w}{\partial z}=0 \\ u|_{z=0}=v|_{z=0}=\dfrac{\partial u}{\partial s}+\dfrac{\partial v}{\partial z}=0 \end{cases} \tag{4-a}$$

$$\begin{cases} 2\int_{-\pi/2}^{\pi/2} SR_m\cos\theta d\theta = F \\ \sigma|_{z=l}=0 \end{cases} \qquad (z=l) \tag{4-b}$$

where u, v and w are the axial, tangent and radial displacements of the flexible ring, respectively, F is the force from the movable tooth. The boundary conditions are: (1) at z=0, change of the principal curvature of the flexible ring in s direction is zero, the strain of the flexible ring in s

direction is zero, the normal stress distributed linearly, the shearing strain and the displacements on the central plane of the flexible ring are zero; (2) at $z=l$, the normal stress is zero, the sum of the shear force is equal to outer load F.

Considering the second equation of Eq. (4-b), the solutions of Eq. (1) can be given by

$$\sigma = \left(1-\frac{z}{l}\right)\left(a_1 \sin\theta + a_2 \cos\theta + a_3\theta + a_4\right) \tag{5-a}$$

$$M = \left(1-\frac{z}{l}\right)\left(b_1 \sin\theta + b_2 \cos\theta + b_3\theta + b_4\right) \tag{5-b}$$

where a_i (i=1,2,3,4) and b_i (i=1,2,3,4) are the undetermined constants, l shows the position of the force F.

Substituting Eq. (5-a) into Eq. (1), and considering the third equations of Eq. (4-a), we obtain

$a_1 = \dfrac{Fl}{\pi R_m{}^2 \delta}$ and $a_2 = a_3 = a_4 = 0$

Thus, Eq. (5-a) can be changed into following form

$$\sigma = \left(1-\frac{z}{l}\right)\frac{Fl}{\pi R_m{}^2 \delta}\sin\theta \tag{6}$$

For Eq. (5-b), considering the symmetry condition of the torque with the plane $\theta=\pi/2$, we obtain

$$b_2 = b_3 = b_4 = 0$$

$$M = \left(1-\frac{z}{l}\right)b_1 \sin\theta \tag{7}$$

Substituting Eq. (7) into the third and fourth equations of Eq. (2) yields

$$\left.\begin{aligned} T &= \left(1-\frac{z}{l}\right)\frac{b_1}{R_m}\sin\theta \\ Q &= \left(1-\frac{z}{l}\right)\frac{b_1}{R_m}\cos\theta \end{aligned}\right\} \tag{8}$$

Substituting Eq. (6) and the first equation of Eq. (8) into the third equation of Eq. (3), yields

$$w = \frac{1}{R_m}\left(\frac{\mu b_1}{E\delta R_m} - \frac{Fl}{\pi E \delta R_m^2}\right)\left(\frac{z^3}{6l} - \frac{z^2}{2}\right)\sin\theta + f_1(s)\,z + f_2(s) \tag{9}$$

Where $f_1(s)$ and $f_2(s)$ are the undetermined functions.

Substituting Eq. (9) and the first and the second equations of Eq. (4-a), yields

$$f_1''(s) + \frac{f_1(s)}{R_m^2} = 0 \tag{10-a}$$

$$f_2''(s) + \frac{f_2(s)}{R_m^2} = 0 \tag{10-b}$$

Combining Eqs. (10) with (9), we can obtain

$$w=\frac{1}{R_m}\left(\frac{\mu b_1}{E\delta R_m}-\frac{Fl}{\pi E\delta R_m^2}\right)\left(\frac{z^3}{6l}-\frac{z^2}{2}\right)\sin\theta+\left(c_1\sin\theta+c_2\cos\theta\right)z+c_3\sin\theta+c_4\cos\theta \tag{11}$$

Substituting Eq. (11) into the fourth equation of Eq. (4a), yields c_i=0. Thus

$$w=\frac{1}{R_m}\left(\frac{\mu b_1}{E\delta R_m}-\frac{Fl}{\pi E\delta R_m^2}\right)\left(\frac{z^3}{6l}-\frac{z^2}{2}\right)\sin\theta \tag{12}$$

In a same manner as Eq. (12), we can obtain equations for displacements *u* and *v*. Substituting Eq. (6) and the first equation of Eq. (8) into the first equation of Eq. (3), yields

$$u=-z\left(\frac{\mu b_1}{E\delta R_m}-\frac{Fl}{\pi E\delta R_m^2}\right)\left(1-\frac{z}{2l}\right)\sin\theta+f_3(s) \tag{13}$$

Substituting Eq. (13) into the fifth equation of Eq. (4a), yields $f_3(s)$=0. Thus

$$u=-z\left(\frac{\mu b_1}{E\delta R_m}-\frac{Fl}{\pi E\delta R_m^2}\right)\left(1-\frac{z}{2l}\right)\sin\theta \tag{14}$$

Substituting Eq. (6) and the first equation of Eq. (8) into the second equation of Eq. (3), yields

$$v=\frac{1}{R_m}\left(\frac{\mu b_1}{E\delta R_m}-\frac{Fl}{\pi E\delta R_m^2}\right)\left(\frac{z^3}{6l}-\frac{z^2}{2}\right)\cos\theta+f_4(s)z+f_5(s) \tag{15}$$

Substituting Eq. (15) into the fifth equation of Eq. (4a), yields $f_4(s)= f_5(s)$=0. Thus

$$v=\frac{1}{R_m}\left(\frac{\mu b_1}{E\delta R_m}-\frac{Fl}{\pi E\delta R_m^2}\right)\left(\frac{z^3}{6l}-\frac{z^2}{2}\right)\cos\theta \tag{16}$$

Substituting Eqs. (7), (12) and (16) into the first equation of Eq. (2), yields

$$\left(1-\frac{z}{l}\right)\left[b_1\sin\theta+\frac{D\mu\sin\theta}{R_m}\left(\frac{Fl}{\pi ER_m^2\delta}-\frac{\mu b_1}{ER_m\delta}\right)\right]=0 \tag{17}$$

From Eq. (17), we give

$$b_1=\frac{\mu FDl}{\pi R_m\left(D\mu^2-E\delta R_m^2\right)}$$

Thus

$$M=\frac{\mu FDl}{\pi R_m\left(D\mu^2-ER_m^2\delta\right)}\left(1-\frac{z}{l}\right)\sin\theta \tag{18}$$

$$\left.\begin{aligned} u &= \frac{Flz}{\pi\left(ER_m^2\delta - D\mu^2\right)}\left(1-\frac{z}{2l}\right)\sin\theta \\ v &= \frac{Fl}{\pi R_m\left(ER_m^2\delta - D\mu^2\right)}\left(\frac{z^3}{6l}-\frac{z^2}{2}\right)\cos\theta \\ w &= \frac{Fl}{\pi R_m\left(D\mu^2 - ER_m^2\delta\right)}\left(\frac{z^3}{6l}-\frac{z^2}{2}\right)\sin\theta \end{aligned}\right\} \tag{19}$$

From Eq. (19), the relationship between the load applied to the flexible ring at $z=l$ and the radial displacement w_l at $z=l$ can be given

$$\frac{F}{\pi R_m\left(ER_m^2\delta - D\mu^2\right)} = \frac{3w_l}{l^3} \qquad (z=l) \tag{20}$$

Thus, the displacements of the flexible ring under jth tooth mesh force can be given

$$\left.\begin{aligned} u_j &= \frac{3R_m z}{l^2}\left(1-\frac{z}{2l}\right)w_l\sin(\theta+\theta_j) \\ v_j &= \frac{3z^2}{2l^2}\left(1-\frac{z}{3l}\right)w_l\cos(\theta+\theta_j) \\ w_j &= \frac{3z^2}{2l^2}\left(1-\frac{z}{3l}\right)w_l\sin(\theta+\theta_j) \end{aligned}\right\} \tag{21}$$

The radial displacement of the flexible ring at $z=l$ is dependent on the motion position of the movable tooth. It can be expressed as

$$w_l = \sqrt{x_j^2+y_j^2} - \sqrt{x_0^2+y_0^2} \qquad (j=1,\ 2,\ 3,) \tag{22}$$

where x_j and y_j are the position coordinates of the movable tooth, x_0 and y_0 are the initial position coordinates of the movable tooth.

The coordinates x_j and y_j of the movable tooth can be given by Qu (2003)

$$\begin{cases} x_j = a\cos\left(i(\varphi_{21}+j\varphi_B)\right) + (R+r)\cos\left((\varphi_{21}+j\varphi_B) - \arcsin\left[a\sin\left((i-1)(\varphi_{21}+j\varphi_B)\right)/(R+r)\right]\right) \\ y_j = a\sin\left(i(\varphi_{21}+j\varphi_B)\right) + (R+r)\sin\left((\varphi_{21}+j\varphi_B) - \arcsin\left[a\sin\left((i-1)(\varphi_{21}+j\varphi_B)\right)/(R+r)\right]\right) \end{cases} \tag{23}$$

where $\varphi=\varphi_{21}+j\varphi_B$ is the angle position of the j*th* movable tooth, φ_B is the tooth distance angle, i is the speed ratio of the motor, it is defined as the ratio of the rotating speed of the voltage to the rotor speed, R is the flexible ring diameter, r is the movable tooth radius, a is the eccentric center distance.

Substituting Eqs. (22) and (23) into (21), yields

$$\begin{cases} w_j = \dfrac{3z^2}{2l^2}\left(\dfrac{z}{3l}-1\right)\cdot(m-n)\cdot\sin\left(\theta+\theta_j\right) \\ v_j = \dfrac{3z^2}{2l^2}\left(1-\dfrac{z}{3l}\right)\cdot(m-n)\cdot\cos\left(\theta+\theta_j\right) \\ u_j = \dfrac{3Rz}{l^2}\left(1-\dfrac{z}{2l}\right)\cdot(m-n)\cdot\sin\left(\theta+\theta_j\right) \end{cases} \tag{24}$$

where $\theta_j = \dfrac{b\pi}{Z} - \left(\dfrac{2\left(\dfrac{\lfloor k \rfloor + 1}{2} \right)}{Z} - \dfrac{k}{Z(Z-1)} \right) \pi$

$$m = \sqrt{a^2 + (R+r)^2 + 2a(R+r)\cos\left((i-1)\varphi_0 + \arcsin\left[\frac{a}{R+r} \sin\left((i-1)\varphi_0 \right) \right] \right)}$$

$$n = \sqrt{a^2 + (R+r)^2 + 2a(R+r)\cos\left((i-1)\varphi + \arcsin\left[\frac{a}{R+r} \sin\left((i-1)\varphi \right) \right] \right)}$$

$$\varphi = \frac{\pi}{i(i-1)} k + \frac{2\pi}{i}(j-1)$$

$$\varphi_0 = \frac{2\pi}{i}(j-1) + \frac{c\pi}{i(i-1)}$$

$$k = \begin{cases} 2n(n \geq 0), & j = j_0 + \left(\left\lfloor \dfrac{i}{4} \right\rfloor - 1 \right) \\ 2n+1(n \geq 0), & j = j_0 + \left(\left\lfloor \dfrac{i}{4} \right\rfloor \right) \end{cases}$$

$$c = \begin{cases} 0, & 2j - \left(\dfrac{i+1}{2} \right) - 1 \leq 0 \\ 2j - \left(\dfrac{i+1}{2} \right) - 1, & 2j - \left(\dfrac{i+1}{2} \right) - 1 > 0 \end{cases}$$

$$b = \begin{cases} 4 - 2\left\{ j - \left(\dfrac{\lfloor k \rfloor}{2} \right) - 1 \right\}, & j = j_0 + \left(\left\lfloor \dfrac{i}{4} \right\rfloor - 1 \right) \\ 6 - 2\left\{ j - \left(\dfrac{\lfloor k \rfloor}{2} \right) - 1 \right\}, & j = j_0 + \left(\left\lfloor \dfrac{i}{4} \right\rfloor \right) \end{cases}$$

Here, $\lfloor k \rfloor$ and $\left\lfloor \dfrac{i}{4} \right\rfloor$ are the floor functions of integer part.

In the drive system, the multi-teeth mesh occurs. Letting the tooth number in mesh simultaneously be *m*, the total displacements of the flexible ring under multi-teeth mesh force can be given by

Table 1 Parameters of the drive sytem

flexible ring length l	20 mm	flexible ring thickness δ	0.2 mm
flexible ring diameter R	10.6 mm	eccentric center distance a	0.1mm
movable tooth number Z	15	movable tooth diameter d	2 mm
rigid gear tooth number Z_r	14	Speed ratio i	15

$$\begin{cases} w=\dfrac{3z^2}{2l^2}\left(\dfrac{z}{3l}-1\right)\cdot\displaystyle\sum_{j=\left[\frac{\lceil k\rceil+1}{2}\right]+1}^{j=j+\left\lfloor\frac{i}{4}\right\rfloor-1\left(\left\lceil\frac{i}{4}\right\rceil-1\right)}\left[(m-n)\cdot\sin\left(\theta+\theta_j\right)\right] \\ v=\dfrac{3z^2}{2l^2}\left(1-\dfrac{z}{3l}\right)\cdot\displaystyle\sum_{j=\left[\frac{\lceil k\rceil+1}{2}\right]+1}^{j=j+\left\lfloor\frac{i}{4}\right\rfloor-1\left(\left\lceil\frac{i}{4}\right\rceil-1\right)}\left[(m-n)\cdot\cos\left(\theta+\theta_j\right)\right] \\ u=\dfrac{3Rz}{l^2}\left(1-\dfrac{z}{2l}\right)\cdot\displaystyle\sum_{j=\left[\frac{\lceil k\rceil+1}{2}\right]+1}^{j=j+\left\lfloor\frac{i}{4}\right\rfloor-1\left(\left\lceil\frac{i}{4}\right\rceil-1\right)}\left[(m-n)\cdot\sin\left(\theta+\theta_j\right)\right] \end{cases} \tag{25}$$

4 Results and discussion

Equations in this paper are utilized for the displacement analysis for the drive system. The parameters of the numerical example are shown in Table 1.

The radial displacements of the flexible ring under multi-teeth mesh force at the ring end (l=20 mm) for the drive system as the function of the rotating angle φ_2 of the rotor and the position angle θ are investigated (see Fig. 4). The axial and tangent displacements of the flexible ring under multi-teeth mesh force at the ring end (l=20 mm) as the function of the rotating angle φ_2 of the rotor and the position angle θ are investigated(see Fig. 5). From Figs. 4-5, it is known:

(1) As the vibrator of the drive system rotates one circle, the rotor rotates one tooth distance (π/7). So, the radial displacements of the flexible ring changes periodically along with the rotation of the vibrator. The change period is one tooth distance (π/7). Fig. 5(a) gives changes of the radial displacements of the flexible ring in one period.

(2) In one tooth distance (π/7), the radial displacements of the flexible ring changes with the rotating angle φ_2 of the rotor. However, there are abrupt changes in radial displacements of the flexible ring at some points where there are abrupt changes in the number of the mesh teeth pair. For instance, at φ_2=15.4°, the radial displacements of the some points of the flexible ring grow abruptly, and the radial displacements of the other points drop abruptly.

(3) Besides the abrupt change points of the mesh teeth pair, the radial displacements of the flexible ring change gradually with the rotating angle φ_2. The maximum displacement of the flexible ring occurs at the position corresponding to the maximum dynamic displacement of the vibrator.

(4) The axial and tangent displacements of the flexible ring change with the rotating angle φ_2. There are also abrupt changes in axial and tangent displacements of the flexible ring at some points where there are abrupt changes in the number of the mesh teeth pair. The displacement distributions are similar to one of the radial displacement. The displacements for the more teeth pairs in mesh are larger than those for the less teeth pairs in mesh. Of course, the positions of the maximum axial and tangent displacements are different from one of the radial displacement.

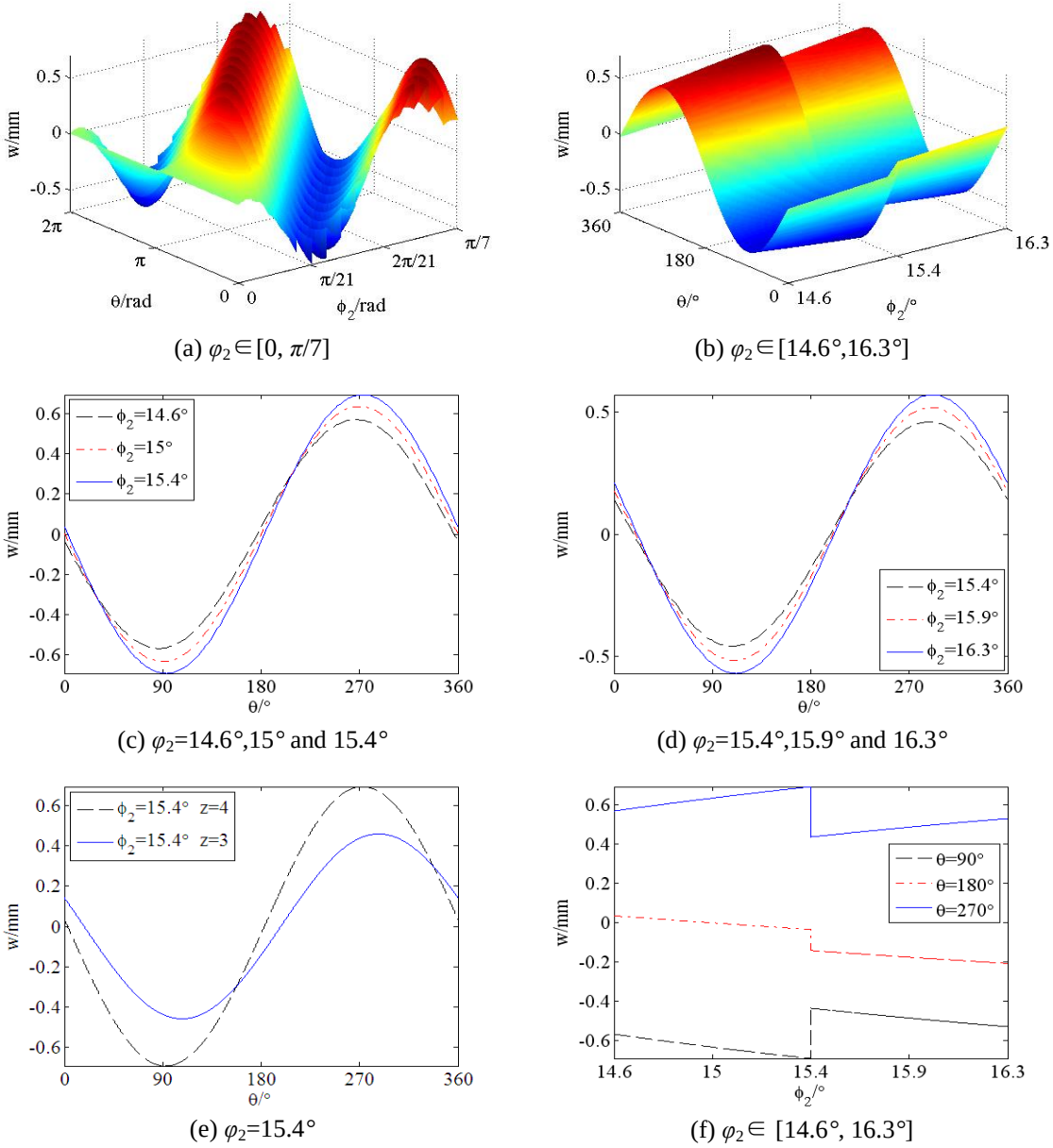

(a) $\varphi_2 \in [0, \pi/7]$ (b) $\varphi_2 \in [14.6°,16.3°]$

(c) φ_2=14.6°,15° and 15.4° (d) φ_2=15.4°,15.9° and 16.3°

(e) φ_2=15.4° (f) $\varphi_2 \in$ [14.6°, 16.3°]

Fig. 4 The radial displacement of the flexible ring under multi-teeth mesh force(l=20mm, ring end)

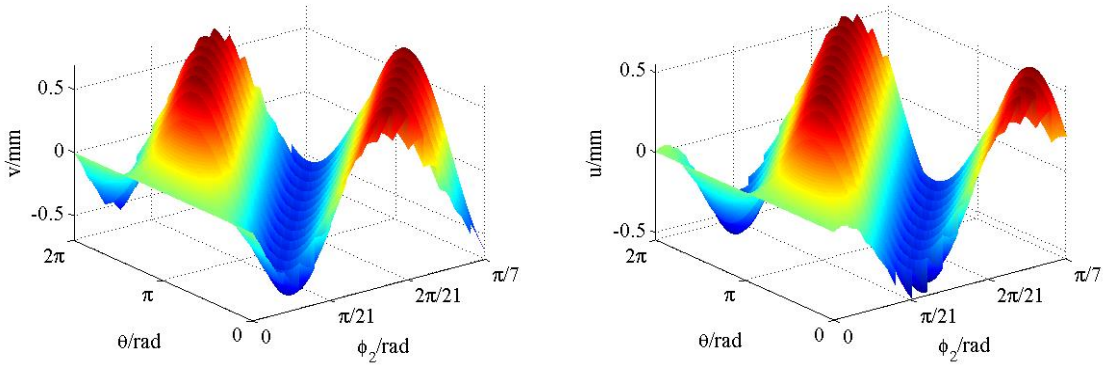

(a) Tangent displacement (b) Axial displacement

Fig. 5 The axial and tangent displacements of the flexible ring under multi-teeth mesh force

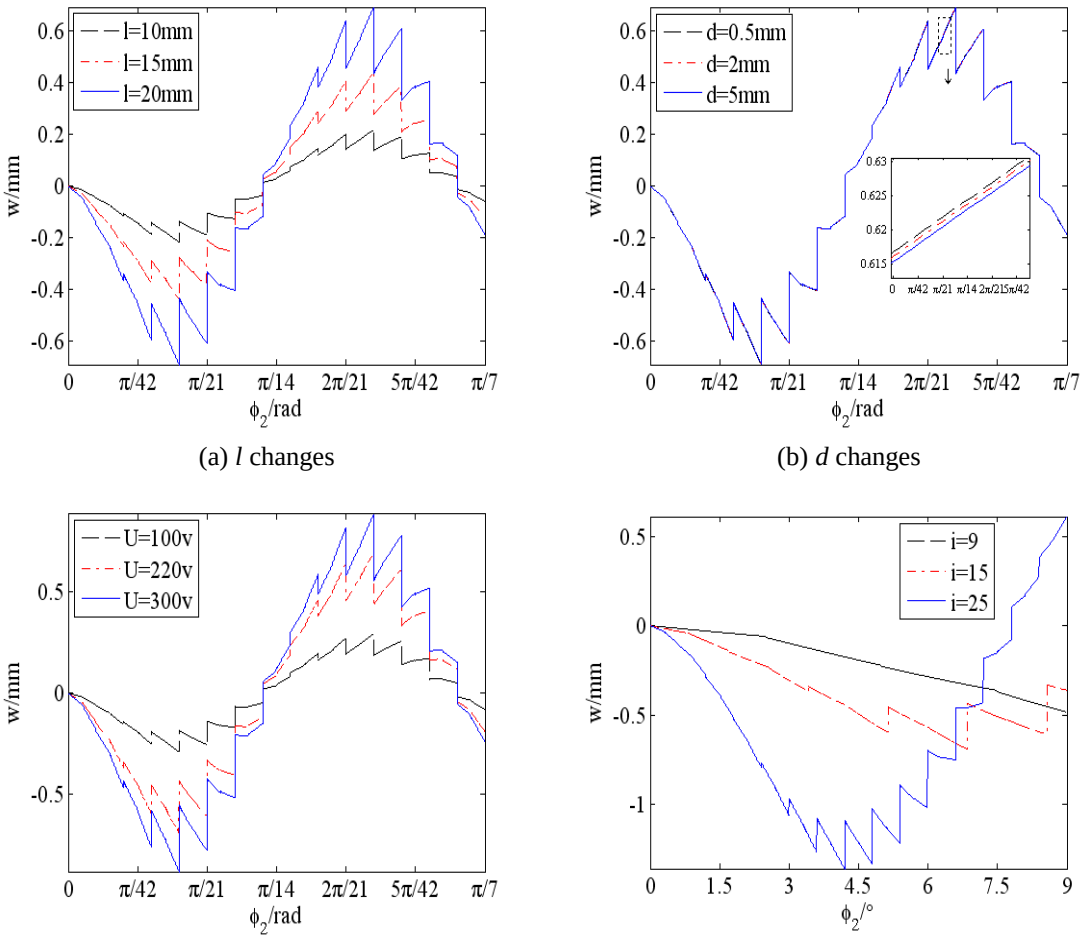

(a) *l* changes (b) *d* changes

(c) *U* changes (d) *i* changes

Fig. 6 Changes of the radial displacements of the flexible ring along with the main parameters

The changes of the radial displacements of the flexible ring along with the main parameters are investigated (see Fig. 6, here $z=l$ and θ=321.4°) From Fig. 6, it is known:

(1) As the length of the flexible ring grows, the radial displacements of the flexible ring grow significantly. There are more abrupt changes in radial displacements of the flexible ring for a larger length of the flexible ring. The large radial displacement of the flexible ring is favorable for the operation of the drive system, but the large fluctuation of the radial displacement will cause dynamic response of the drive system. So, a moderate length of the flexible ring should be taken.

(2) As the diameter of the movable tooth (ball) grows, the radial displacements of the flexible ring drop slightly. It shows that the diameter of the ball has little effects on the radial displacements of the flexible ring.

(3) As the excitation voltage of the piezoelectric ceramics grows, the radial displacements of the flexible ring grow significantly. As the excitation voltage of the piezoelectric ceramics grows, the fluctuation of the radial displacements of the flexible ring also grows significantly. For the excitation voltage larger than 200V, the increase of the radial displacements with the voltage is obviously smaller than that for the excitation voltage below 200V. So, the excitation voltage should be taken as the values below 200V.

(4) As the speed ratio of the drive system grows, the radial displacements of the flexible ring grow significantly, and the fluctuations of the radial displacements also grow significantly. However, the fluctuation period of the radial displacements drops obviously with increasing the speed ratio. The fluctuation frequency of the radial displacements should be taken to be different from the natural frequency of the drive system.

5. Conclusions

In this paper, an electromechanical integrated harmonic piezodrive system is proposed in which the piezodrive principle is combined with the harmonic drive and the movable tooth drive principles, and a reduction ratio is realized. It can cause a significant increase of the output torque as well as increase of the operating life and efficiency. The operating principle is introduced. The equation of the relationship between the displacements of the flexible ring and the rotating angle of the rotor is deduced. Using the equation, the displacements of the flexible ring for the drive system and their changes along with the system parameters are investigated. The results show:

- The displacements of the flexible ring changes periodically along with the rotation of the vibrator. The change period is one tooth distance.
- There are abrupt changes in the displacements of the flexible ring at some points where there are abrupt changes in the number of the mesh teeth pair.
- The length of the flexible ring, the excitation voltage, and the speed ratio has obvious effects on the displacements of the flexible ring.

AcknowledgmentS

This work is supported by National Natural Science Foundation of China (51275441).

References

Hieu, N.T., Odomari, S. and Yoshida, T. (2013), "Nonlinear adaptive control of ultrasonic motors considering dead-zone", *IEEE Tran. Indus. Inform.*, **9**(4), 1847-1854.

Hojjat, Y. and Karafi, M.R. (2010), "Introduction of roller interface ultrasonic motor", *Sens. Actuat. A*, **163**(1), 304-310.

Qu, J.F. (1993), *Movable tooth drive theory*, Mechanical Industrial Press, Beijing. China. (in China)

Rho, J.S., Lee, C.H. and Jung, H.K. (2008), "Characteristic analysis and design of a small size rotary ultrasonic motor using the cutting method", *Int. J. Appl. Electrom. Mech.*, **28**(4), 469-500.

Sashida, T. (1982), "Trial construction and operation of an ultrasonic vibration driven motor", *Oyo Butsiuri*, **51**(6), 713-718.

Sashida, T. (1984), "Motor device utiliaing ultrasonic oscillation", *US Patent*, 4562374.

Shi, J.Z. and You, D.M. (2014), "Characteristic model of travelling wave ultrasonic motor", *Ultrasonics*, **54**(2), 725-730.

Stepanenko, D.A. and Minchenya, V.T. (2012), "Development and study of novel non-contact ultrasonic motor based on principle of structural asymmetry", *Ultrasonics*, **52**(7),866-872.

Tokushima, A. and Harao, N. (1987), "Ultrasonic motor", *Nat. Tech. Report*, **33**, 542-550. (in Japan)

Ueha, S., Hashimoto, Y. and Koike, Y. (2000), "Non-contact transportation using near-field acoustic levitation", *Ultrasonics*, **38**(1-8), 26-32.

Xu, L.Z. and Li, H.Y. (2013), "Free vibration for an electromechanical integrated harmonic piezodrive system", *Int. J. Appl. Electrom. Mech.*, **42**(2), 269-282.

Yamayoshi, Y. and Hirose, S. (1992), "Ultrasonic motor not using mechanical friction force", *Int. J. Appl. Electrom. Mech.*, **3**, 179-182.

Yang, B., Liu, J.Q. and Chen, D. (2006), "Theoretical and experimental research on a disk-type non-contact ultrasonic motor", *Ultrasonics*, **44**(3), 238-240.

CC